

Smartphone Inertial Sensors in Gait Analysis: A Comparison with a Commercial Device

Marco Oliveira¹^a, William Fröhlich¹^b, Rafael Baptista¹^c, Sandro Rigo²^d and César Marcon¹^e

¹*School of Technology, Pontifical Catholic University of Rio Grande do Sul (PUCRS), Porto Alegre, Brazil*

²*Universidade do Vale do Rio dos Sinos (UNISINOS), São Leopoldo, Brazil*

Keywords: Gait, Inertial Sensors, Biomechanics, Smartphone, Wearable Sensors.

Abstract: Human gait analysis is a crucial tool in healthcare, providing valuable insights into an individual's well-being, as various disorders and diseases can be detected through changes in walking patterns. This study aims to validate the gait sensing results obtained from a smartphone, an easily accessible and portable device, by comparing them with equivalent data from the G-Walk, a widely used commercial equipment. The goal is to assess the applicability and accuracy of the solution with the support of healthcare professionals, ensuring its effectiveness in clinical settings.

1 INTRODUCTION

This paper presents a detailed investigation of using inertial sensors embedded in smartphones, such as accelerometers and gyroscopes, for human gait analysis. The study compares the sensing results obtained from a smartphone with those obtained from a commercial device, specifically the G-Walk (BTS Bioengineering, 2024) system, a widely recognized tool for biomechanics assessments. Our validation goal is to determine whether smartphone data can be utilized to develop an algorithm capable of analyzing gait patterns, serving as a reliable substitute for established tools.


G-Walk is used in clinical settings to evaluate movement and gait, serving as a benchmark for reliability in motion analysis. The validation developed during this paper focuses on assessing the comparability of data collected by the smartphone with G-Walk measurements across various parameters. If smartphones provide sufficiently accurate data for the future development of algorithms designed for gait pattern recognition, they could enable routine monitoring of gait-related health conditions in everyday settings, transforming how gait analysis is performed and expanding its applications in healthcare.


2 RELATED WORK


Gait analysis is a valuable tool in healthcare, traditionally relying on methods such as optical motion capture systems, force platforms, and pressure sensors. While these methods are considered highly accurate, they are often expensive and require specialized setups that normally involve complex data processing, limiting their use outside clinical environments (Hausdorff and Alexander, 2005).


Wearable technologies and smartphones, however, typically feature embedded Inertial Measurement Units (IMUs)—accelerometers and gyroscopes—which serve as affordable and portable alternatives for gait analysis. Their accessibility allows for broader use beyond clinical settings. Research has demonstrated that smartphone accelerometer and gyroscope data can yield gait analysis results comparable to those produced by traditional methods (Caro-Alvaro et al., 2024).


The quality of data from smartphone sensors can significantly impact the accuracy of gait analysis. To mitigate this, preprocessing techniques such as noise filtering, signal normalization, and feature extraction are applied to make raw sensor data more usable. Standard filtering methods, like the Kalman filter, help reduce noise (Kim et al., 2018), while frequency-domain techniques such as the Fourier Transform aid in identifying gait patterns within acceleration data (Shi et al., 2023). Additionally, studies have shown the effectiveness of preprocessing across various walking conditions and sensor placements (Arshad et al., 2022) (Ramli et al., 2024).

^a  <https://orcid.org/0009-0003-7625-0735>

^b  <https://orcid.org/0000-0003-3551-2623>

^c  <https://orcid.org/0000-0003-1937-6393>

^d  <https://orcid.org/0000-0001-8140-5621>

^e  <https://orcid.org/0000-0002-7811-7896>

Machine learning techniques have further enhanced gait analysis by enabling the automated detection of gait events. Commonly used algorithms in this field include Convolutional Neural Networks (CNNs) and Long Short-Term Memory (LSTM) networks, which are particularly well-suited for analyzing time-series sensor data. LSTM networks, in particular, can outperform traditional techniques in recognizing gait phases (Huang et al., 2021) (Marimon et al., 2024), and combining CNNs with LSTM networks has proven effective in classifying complex gait patterns (Das et al., 2022).

While techniques used in G-Walk (BTS Bioengineering, 2024) offer highly detailed data using specialized hardware, smartphone-based gait analysis aims to replicate this precision at a lower cost. Previous studies have found that calibrated smartphone sensors can closely match the performance of widely used commercial equipment when used under controlled conditions (Lopez-Nava et al., 2020). However, several challenges remain for smartphone-based gait analysis to achieve the accuracy of traditional methods. Factors such as variations in sensor quality across smartphone models, noise from different sensor attachment methods, and environmental influences like walking speed or uneven surfaces can affect the results. Ongoing validation, calibration, and algorithm improvements are necessary to ensure the reliability of smartphone-based gait analysis in real-world scenarios (Kocuvan et al., 2023).

This study builds on previous research by comparing smartphone sensor data with the G-Walk system to assess the viability of smartphones as data-gathering tools for gait monitoring.

3 MATERIALS AND METHODS

This section outlines the data collection, processing, and analysis procedure to ensure the study follows a robust methodological framework. All essential elements were carefully addressed to enable the validation of the smartphone-based method as a reliable alternative to established systems used in gait analysis.

3.1 Sensors Specifications

Comparing the hardware specifications of the sensors was essential for an initial compatibility evaluation, ensuring that both devices have a similar capacity for capturing data. This subsection presents the main specifications of the sensors.

The 'device info' function in Phyphox (Staaacks et al., 2018) was used to discover the hardware con-

tained in the smartphone. The main sensor is the LSM6DSO from STMicroelectronics. Its specifications are as follows (STMicroelectronics, 2024):

- **Accelerometer:** 16-bit/axis triaxial accelerometer with a full-scale range of ± 2 , ± 4 , ± 8 , ± 16 g
- **Gyroscope:** 16-bit/axis triaxial gyroscope with a full-scale range of ± 125 , ± 250 , ± 500 , ± 1000 , ± 2000 $^{\circ}/s$

The *G-Walk* has three main sensors, but since this paper does not address the usage of the magnetometer, the specifications of the two sensors used are as follows (BTS Bioengineering, 2024):

- **Accelerometer:** 16-bit/axis triaxial accelerometer with a full-scale range of ± 2 , ± 4 , ± 8 , ± 16 g
- **Gyroscope:** 16-bit/axis triaxial gyroscope with a full-scale range of ± 250 , ± 500 , ± 1000 , ± 2000 $^{\circ}/s$

An initial evaluation shows that both devices have identical accelerometer hardware specifications. However, the main difference for the gyroscope is that the LSM6DSO is better suited for measuring low-speed rotations, as it offers an additional range of ± 125 degrees per second.

3.2 Data Gathering

The initial step involved collecting raw gait data from our reference commercial system using inertial sensors from both the smartphone and G-Walk.

The smartphone application Phyphox (Staaacks et al., 2018) captures linear acceleration and angular velocity. Phyphox is an open-source tool developed by RWTH Aachen University, allowing access to all available sensor data on smartphones. The primary sensors used in this study include accelerometers, which measure linear acceleration (in m/s^2), and gyroscopes, which measure angular velocity (in $^{\circ}/s$).

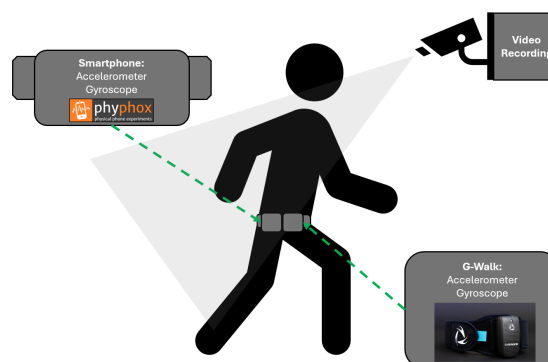


Figure 1: Methodology used in the trial.

Figure 1 shows that both devices—the smartphone and G-Walk—were mounted on the subject's waist

using a running belt. This placement was selected because it is the standard position for using the G-Walk system, allowing for direct comparisons. Additionally, it ensures consistency in the data collection process, as this location effectively captures hip motion. Both devices recorded data simultaneously while walking to minimize variations caused by separate data collection sessions.

The trial consisted of a single subject walking regularly along a straight path. It lasted approximately 40 seconds, during which 60 steps were recorded. This number was determined empirically by analyzing a video recorded during data collection. The video was also used for time synchronization purposes.

The data was saved in a structured format. Phyphox generated a spreadsheet containing the smartphone data, and the G-Walk system provided a text file with the recorded signals and a report summarizing the gait analysis.

3.3 Preprocessing

Several steps were taken to prepare the data for further analysis, primarily because the data from Phyphox and G-Walk were in different formats. The first step was to ensure compatibility between the datasets by renaming columns, converting units, and ensuring consistent time references.

The initial timestamps were discrepant since the recordings were manually started on both devices. An offset correction was applied to align the timestamps, ensuring both datasets had a common structure for more straightforward analysis. Additionally, an extra offset adjustment was made to ensure that the zero level of each axis was consistent across both datasets.

Following the data cleaning and synchronization, some features were calculated from the raw signals. The columns below were added to both datasets:

- **Absolute acceleration** - calculated as the magnitude of the acceleration vector, combining the X, Y, and Z axes;
- **Absolute angular velocity** - similar to absolute acceleration, but for the gyroscope data;
- **Roll, Pitch, and Yaw** - obtained by integrating the angular velocity over time, allowing the analysis of rotational motion.

3.4 Visual Comparison

Before conducting a more advanced statistical analysis, a visual comparison was used to evaluate the collected data preliminary. This approach provided an

intuitive way to assess the similarity between the signals captured from the smartphone and those from the G-Walk system.

The primary method involved creating figures to overlay the smartphone and G-Walk time-series data: acceleration and angular velocity. Specific data segments were enlarged to focus on individual gait cycles to facilitate this comparison. These zoomed-in figures provided a closer look at the alignment of peaks and the shape of the waveforms, helping to identify minor differences that might not be as evident in full-length plots. The zoomed-in figure for the accelerometer data is presented in Figure 2, while the zoomed-in figure for the gyroscope data is shown in Figure 3.

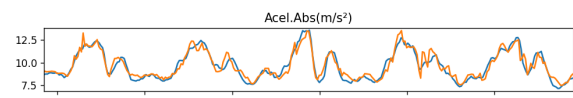


Figure 2: Accelerometer time series zoomed-in.

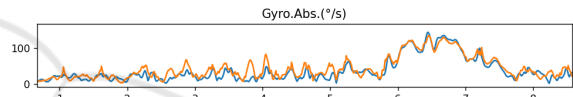


Figure 3: Gyroscope time series zoomed-in.

3.5 Statistical/Hypothesis Test

This section outlines the steps taken for data preprocessing and the statistical methods used to compare the datasets collected by the wearable device and the smartphone.

3.5.1 Data Preprocessing

Initially, the raw data underwent preprocessing to ensure consistency and comparability between the devices. Invalid values recorded during data collection were first removed. Next, interpolation techniques were applied to address missing data (NaN values) and fill gaps in the time series. A low-pass Butterworth filter was then used to eliminate high-frequency noise that could distort the signal and affect the quality of subsequent analyses. The StandardScaler normalization technique was applied to standardize the datasets, ensuring that both were on the same scale, which is critical for meaningful comparisons.

The two devices had different sampling rates, so the datasets were synchronized using a temporal approximation technique. This alignment was essential to ensure that data points from both devices corresponded to the same events in time, allowing for an accurate comparison between the specialized sensors of the wearable device and the general-purpose IMU sensors of the smartphone.

3.5.2 Correlation and Cross-Correlation

We applied correlation techniques to assess the similarity between the data from the two devices. Pearson correlation was used to measure the linear relationship between the datasets. Pearson is ideal when the data follows a normal distribution and a linear relationship between variables is assumed. However, this method is sensitive to outliers, which can disproportionately affect the correlation coefficient, potentially leading to skewed results.

In addition to Pearson, we applied Spearman correlation to evaluate cases where the relationship between variables might not be strictly linear. Spearman is a non-parametric measure of rank correlation, assessing how well the relationship between two variables can be described using a monotonic function. This method does not assume normality or linearity; it is less sensitive to outliers, making it suitable for scenarios where the data might contain anomalies or the relationship between the datasets is non-linear. We captured linear and non-linear relationships between the two data sources by combining Pearson and Spearman correlations.

We also applied cross-correlation to analyze the temporal alignment between the signals. This technique identifies the time shift that maximizes the similarity between the two signals, enabling us to detect potential delays or desynchronization between the devices. This is particularly relevant for cyclic events such as gait, where slight timing discrepancies could affect the data interpretation.

3.5.3 Bland-Altman Analysis

We employed the Bland-Altman analysis to assess the agreement between the wearable and smartphone measurements. This method plots the difference between the two measurements against their mean, allowing for identifying biases and limits of agreement. The Bland-Altman plot is handy for detecting systematic differences (bias) between methods, something that correlation analysis alone may fail to reveal. For instance, even when two methods show high correlation, they may still exhibit a consistent bias, evident in the Bland-Altman plot but not in the correlation coefficient.

3.5.4 Error Analysis: RMSE and MAE

In addition to these qualitative assessments, we quantified the magnitude of the errors between the two devices using Root Mean Square Error (RMSE) and Mean Absolute Error (MAE). RMSE emphasizes more significant deviations by taking the square root

of the average of the squared differences between the two sets of measurements, making it more sensitive to substantial errors. In contrast, MAE provides a straightforward interpretation of the average absolute error, offering a more robust measure in the presence of outliers. These error metrics are crucial for evaluating the overall accuracy of the devices in capturing similar measurements.

3.5.5 Lin's Concordance Correlation Coefficient

To provide a more robust evaluation of concordance between the devices, we also computed Lin's Concordance Correlation Coefficient (CCC). This metric combines measures of correlation and agreement, assessing how closely the measurements from the two devices align in trend and magnitude. Lin's CCC is beneficial when the goal is to determine if the two methods are correlated and if their values are similar in absolute terms.

3.5.6 Fast Fourier Transform Analysis

Lastly, we performed a Fast Fourier Transform (FFT) analysis to compare the frequency content of the signals from both devices. FFT decomposes the time-domain signals into frequency components, enabling us to assess whether the devices captured the same dominant frequencies in the gait cycle. Frequencies related to step cadence and stride patterns are critical for gait analysis. Differences in the frequency components between the two datasets may indicate that the devices are not capturing the movement dynamics with the same precision, which could be necessary depending on the intended application of the data.

4 RESULTS AND DISCUSSION

4.1 Correlation and Cross-Correlation

When analyzing Pearson and Spearman correlations between wearable sensors and smartphones, we observe varying levels of correlation across acceleration variables (*acc*), gyroscope variables (*gyro*), and rotation angles (*roll*, *pitch*, *yaw*).

From an initial analysis using Pearson correlations, as seen in Figure 4, which measures linear relationships between variables, we find high correlations for most acceleration and gyroscope axes. For instance, the absolute acceleration (*acc.abs*) shows a strong correlation of 0.931, suggesting that wearable devices and smartphones similarly capture overall acceleration magnitude. Gyroscope values exhibit even

higher correlations, such as *gyro_x* (0.951), *gyro_z* (0.911), and absolute gyroscope (*gyro_abs*, 0.944), indicating substantial agreement between the sensors in measuring rotational movement. The highest correlations are found in *roll* (0.99996) and *yaw* (0.99976), reflecting a near-perfect agreement in these rotational angles. Yet, a fundamental exception is the low correlation in the Y-axis, particularly for the gyroscope, where *gyro_y* shows a correlation of just 0.165. This suggests a significant discrepancy between the wearable and smartphone measurements on the Y-axis for gyroscope data. The accelerometer on the Y-axis also has the lowest correlation among the acceleration axes but performs significantly better than *gyro_y*, with a Pearson correlation coefficient of 0.779.

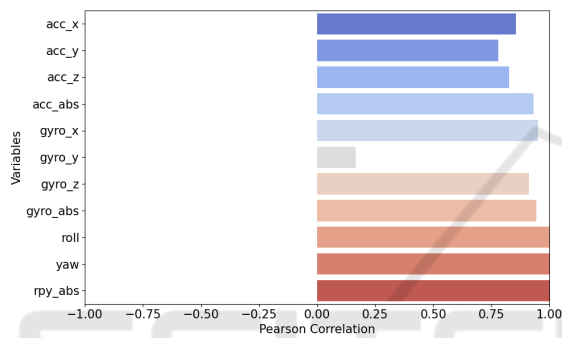


Figure 4: Pearson correlation between wearable sensor and smartphone data across acceleration, gyroscope, and rotation variables.

Figure 5 also displays Spearman correlations, measuring monotonic relationships and generally confirming the patterns observed with Pearson correlations, albeit with some differences.

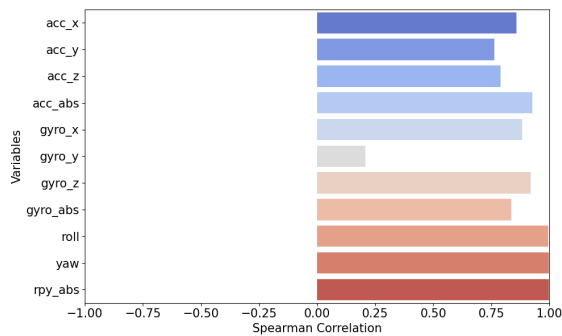


Figure 5: Spearman correlation between wearable sensor and smartphone data across acceleration, gyroscope, and rotation variables.

As expected, the Spearman correlations for acceleration are also high, such as *acc_x* (0.858) and *acc_abs* (0.928), indicating that the overall trend between the two devices remains strong even when

considering non-linear relationships. However, for the gyroscope, Spearman correlations are slightly lower, especially for *gyro_x* (0.884) and *gyro_abs* (0.835), suggesting that the devices may detect rotations differently, particularly when considering non-linear movements.

We observed a consistent pattern in the cross-correlation analysis across all data points analyzed. There was either a low negative or low positive correlation for negative lag values, with values gradually increasing. However, the correlation remained stable at the observed levels for positive lag values, as shown in Figure 6.

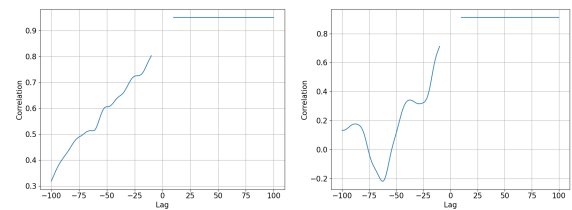


Figure 6: Cross-correlation analysis for *gyro_x* (left) and *gyro_z* (right), showing correlation patterns across lag values.

4.2 Bland-Altman Analysis

Figure 7 displays the results for *acc_x* using the Bland-Altman technique, which assesses the agreement between two measurement methods: a wearable device and a smartphone. The X-axis represents the average of the measurements between the two methods, while the Y-axis shows the difference between these measurements.

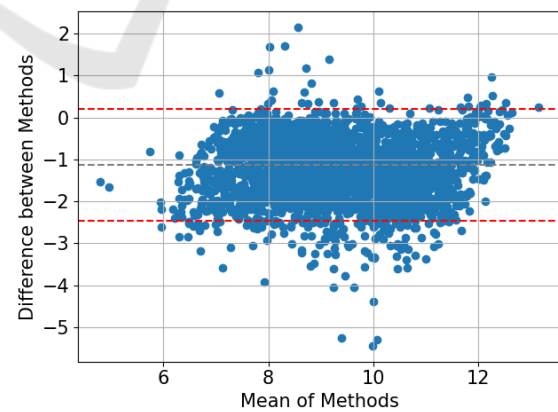


Figure 7: Bland-Altman plot comparing wearable sensor and smartphone measurements for *acc_x*.

The central gray line indicates the mean of the differences, which is slightly below -1. This suggests that the wearable device tends to register slightly lower values than the smartphone, revealing a slight

negative bias, implying that one device may slightly underestimate the values.

The red dashed lines mark the limits of agreement, which range approximately from -3 to +1. Most data points fall within these limits, indicating good agreement between the methods for most of the data. However, a few points fall outside these limits, representing outliers where the devices show more significant disagreement. Hence, both methods demonstrate good agreement on the *acc_x* axis, with a slight negative bias and relatively consistent differences throughout the measurements.

In contrast, Figure 8 analyzes *gyro_y* using the Bland-Altman agreement technique. The central gray line represents the mean of the differences, which is around 0 but shows a slight upward shift. This indicates a small positive bias, suggesting that the wearable device records slightly higher values than the smartphone.

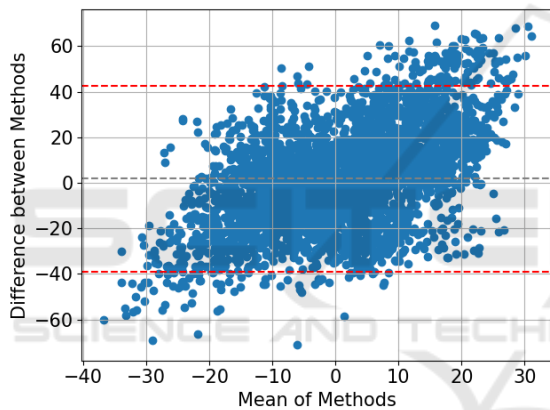


Figure 8: Bland-Altman plot comparing wearable sensor and smartphone measurements for *gyro_y*.

The red dashed lines mark the limits of agreement, encompassing most of the data points. These limits, approximately between -40 and +40, represent the range where most differences are concentrated, with a few outliers falling outside these limits.

Furthermore, the data suggests a proportional bias. The agreement between the two methods is stronger for smaller measurements, but the differences also tend to grow as the average values increase. This divergence is particularly noticeable during faster rotations or larger movements along the *gyro_y* axis, indicating a potential limitation of the wearable device in capturing such movements.

4.3 Error Analysis: MSE, RMSE, and MAE

Table 1 presents the error metrics analyzed in this study, comparing the results from data obtained using a wearable sensor and a smartphone. The table highlights three key error metrics: Mean Absolute Error (MAE), Mean Squared Error (MSE), and Root Mean Squared Error (RMSE).

Table 1: Error metrics (MAE, MSE, RMSE) comparing wearable sensor and smartphone data across various variables.

Variable	MAE	MSE	RMSE
<i>acc_x</i>	0.416	0.286	0.535
<i>acc_y</i>	0.531	0.441	0.664
<i>acc_z</i>	0.455	0.346	0.588
<i>acc_abs</i>	0.248	0.137	0.370
<i>gyro_x</i>	0.237	0.097	0.312
<i>gyro_y</i>	1.005	1.668	1.291
<i>gyro_z</i>	0.335	0.177	0.421
<i>gyro_abs</i>	0.251	0.111	0.333
<i>pitch</i>	1.544	3.349	1.830
<i>roll</i>	0.007	7.712e-05	0.008
<i>yaw</i>	0.018	0.001	0.021
<i>rpy_abs</i>	0.004	3.199e-05	0.005

When analyzing the accelerometer variables, we observe that the absolute acceleration (*acc_abs*) has the lowest errors across all metrics, with an MAE of 0.248, MSE of 0.137, and RMSE of 0.370. This indicates that the overall magnitude of acceleration is well-estimated, demonstrating a solid agreement between the sensors.

Among the individual accelerometer axes, the *acc_x* axis performs slightly better with an MAE of 0.416, followed by the *acc_z* axis with an MAE of 0.455. The *acc_y* axis shows the highest error among the accelerometer axes, with an MAE of 0.531, MSE of 0.441, and RMSE of 0.664, indicating lower precision on this axis.

For the gyroscope variables, the *gyro_x* axis stands out with the lowest errors, showing an MAE of 0.237, MSE of 0.097, and RMSE of 0.312, followed closely by *gyro_abs* with similar values. In contrast, the *gyro_y* axis presents significantly higher errors, with an MAE of 1.005, MSE of 1.668, and RMSE of 1.291, indicating considerable inaccuracy in gyroscope measurements on this axis. This discrepancy reflects a more significant variation between the wearable and smartphone sensors and aligns with the previously analyzed correlation values.

The rotation angles (*pitch*, *roll*, *yaw*) also exhibit error variability. The *roll* angle shows the lowest er-

rors, with minimal values (MAE of 0.007), suggesting almost no discrepancy. The *yaw* angle performs slightly worse, though still very accurate, with an MAE of 0.018. On the other hand, the *pitch* angle has the highest errors among the rotation variables, with an MAE of 1.544, MSE of 3.349, and RMSE of 1.830, indicating more incredible difficulty in estimating this angle.

Overall, the results show strong agreement between the sensors for most variables, with notable exceptions for the *gyro_y* axis and the *pitch* angle, which present higher error levels.

4.4 Lin's Concordance Correlation

Figure 9 depicts the results of the Concordance Correlation Coefficient (CCC) for absolute acceleration (*acc_{abs}*). We have the actual and predicted values on the X and Y axes. Each blue dot corresponds to a pair of actual and predicted values from the dataset, while the red dashed line represents the identity line, which indicates perfect agreement.

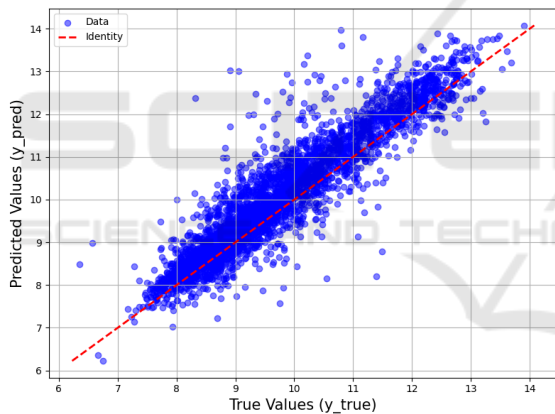


Figure 9: Lin's CCC for absolute acceleration (*acc_{abs}*), showing agreement between wearable sensor and smartphone measurements.

We can discern a strong positive correlation between the actual and predicted values. Most points are clustered around the red identity line, indicating a good fit. However, some variations are present, particularly at the higher and lower extremes, suggesting potential limitations in extreme conditions. The spread of the points suggests a certain degree of variability. Yet, the strong clustering near the identity line reassures us about the model's accuracy in capturing the overall trend, suggesting that the model or sensors perform well but may show limitations in extreme conditions, where predictions deviate slightly from the actual values. Nonetheless, the overall alignment with the identity line indicates good agreement be-

tween the actual and predicted measurements. However, Figure 10 shows a strong correlation between the points. Still, they show a slight offset below the red identity line, indicating that the data does not exhibit a perfect concordance correlation, therefore, there may be variations in magnitude compared to absolute acceleration, demonstrating a closer correlation.

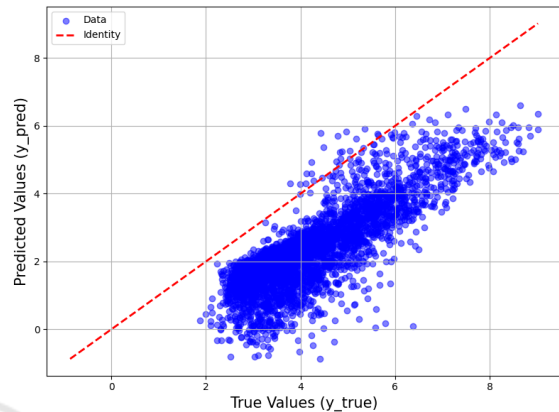


Figure 10: Lin's CCC for *acc_z*, showing slight deviations from the identity line.

4.5 Fast Fourier Transform Analysis

Figure 11 shows the first analysis with the FFT applied to *acc_x*. We observed a very sharp peak around 0 Hz in magnitude and frequency, indicating a dominant frequency component near zero and predominantly low-frequency components, with minimal variation in magnitude outside the central peak. This suggests that the accelerometer's X-axis data contains a significant DC component or a slow-moving trend. The accelerometer on the X-axis may be sensing minimal or constant motion over time, leading to this dominant low-frequency component. The sharp peak near 0 Hz implies that both datasets recorded minimal acceleration on the X-axis, indicating little to no significant movement or only slow changes.

Figure 12 displays the second signal analyzed - *gyro_y*. This figure shows more distributed peaks centered around 0 Hz, with visible spikes across the frequency range. We identified higher frequencies, indicating more variability or dynamic activity in the gyroscope's Y-axis data. The signal's amplitude is also more spread, suggesting that the gyroscope detected rotational movements oscillating at different frequencies. This could result from rotational motion or orientation changes, causing the gyroscope's Y-axis to pick up varying frequencies. Both devices recorded rotational movements on the Y-axis but with different frequency components.

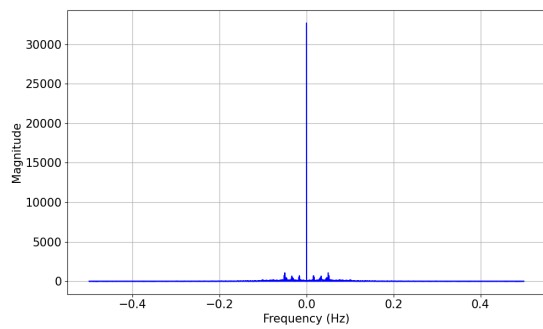


Figure 11: FFT analysis of *acc_x* from wearable sensor and smartphone data, showing the frequency spectrum.

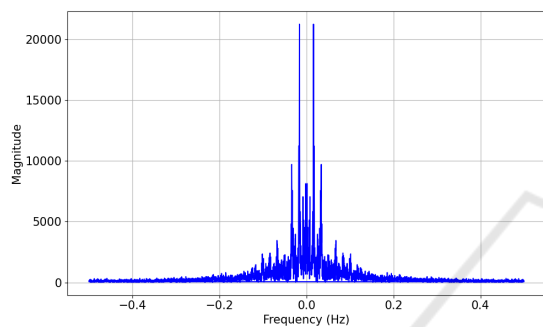


Figure 12: FFT analysis of *gyro_y* from wearable sensor and smartphone data, showing dynamic movement across frequencies.

5 CONCLUSION

Linear correlation provides an overview of relationships between signals but lacks precision in evaluating agreement. In contrast, Bland-Altman plots and Lin's Concordance Correlation Coefficient offer a more robust assessment, essential for validating methods in clinical and biomechanical studies. Error metrics like RMSE and MAE quantify discrepancies, while FFT confirms whether devices capture critical motion frequencies similarly.

Our findings demonstrate that smartphones with inertial sensors are highly promising for gait analysis. They showed strong correlations with the G-Walk system for variables like absolute acceleration (*acc_abs*) and gyroscope data (*gyro_abs*). Bland-Altman analysis revealed satisfactory agreement overall, though notable discrepancies in the gyroscope Y-axis (*gyro_y*) highlight limitations in capturing specific rotational movements. Error metrics confirmed these results, with minimal errors in absolute acceleration and larger discrepancies in *gyro_y*. FFT analysis validated the smartphone's ability to represent essential gait cycle phases accurately.

This study establishes smartphones as accessible

alternatives for gait analysis, though improving Y-axis gyroscope accuracy is critical for complete interchangeability. Future work should focus on developing algorithms to analyze accelerometer and gyroscope data, identify gait phases, and generate detailed reports for healthcare professionals.

REFERENCES

- Arshad, M., Jamsrandorj, A., Kim, J., and Mun, K.-R. (2022). Gait events prediction using hybrid cnn-rnn-based deep learning models through a single waist-worn wearable sensor. *Sensors*, 22(21):8226.
- BTS Bioengineering (2024). G-walk: Wearable inertial sensor for motion analysis.
- Caro-Alvaro, S., Garcia-Lopez, E., et al. (2024). Gesture-based interactions: Integrating accelerometer and gyroscope sensors in the use of mobile apps. *Sensors*, 24(3):1004.
- Das, S., Meher, S., and Sahoo, U. K. (2022). A unified local-global feature extraction network for human gait recognition using smartphone sensors. *Sensors*, 22(11):3968.
- Hausdorff, J. and Alexander, N. (2005). *Gait disorders evaluation and management*. CRC Press.
- Huang, H., Zhou, P., Li, Y., and Sun, F. (2021). A lightweight attention-based cnn model for efficient gait recognition with wearable imu sensors. *Sensors*, 21(8):2866.
- Kim, Y., Bang, H., et al. (2018). Introduction to kalman filter and its applications. *Introduction and Implementations of the Kalman Filter*, 1:1–16.
- Kocuvan, P., Hrastič, A., Kareska, A., and Gams, M. (2023). Predicting a fall based on gait anomaly detection: a comparative study of wrist-worn three-axis and mobile phone-based accelerometer sensors. *Sensors*, 23(19):8294.
- Lopez-Nava, I. H., Valentín-Coronado, L. M., Garcia-Constantino, M., and Favela, J. (2020). Gait activity classification on unbalanced data from inertial sensors using shallow and deep learning. *Sensors*, 20(17):4756.
- Marimon, X., Mengual, I., et al. (2024). Kinematic analysis of human gait in healthy young adults using imu sensors: exploring relevant machine learning features for clinical applications. *Bioengineering*, 11(2):105.
- Ramli, A., Liu, X., , et al. (2024). Gait characterization in duchenne muscular dystrophy (dmd) using a single-sensor accelerometer: classical machine learning and deep learning approaches. *Sensors*, 24(4):1123.
- Shi, L.-F., Liu, Z.-Y., Zhou, K.-J., Shi, Y., and Jing, X. (2023). Novel deep learning network for gait recognition using multimodal inertial sensors. *Sensors*, 23(2):849.
- Staacks, S., Hütz, S., Heinke, H., and Stampfer, C. (2018). Advanced tools for smartphone-based experiments: phyphox. *Physics education*, 53(4):045009.
- STMicroelectronics (2024). Lsm6ds0. Acessado em: 20 de outubro de 2024.